Effects of phase coherence on local density of states in superconducting proximity structures

Shu-Ichiro Suzuki,[1,2] Alexander A. Golubov,[2,3] Yasuhiro Asano,[3,4,5] and Yukio Tanaka[1]

[1]*Department of Applied Physics, Nagoya University, Nagoya 464-8603, Japan*
[2]*MESA$^+$ Institute for Nanotechnology, University of Twente, 7500 AE Enschede, The Netherlands*
[3]*Moscow Institute of Physics and Technology, 141700 Dolgoprudny, Russia*
[4]*Department of Applied Physics, Hokkaido University, Sapporo 060-8628, Japan*
[5]*Center of Topological Science and Technology, Hokkaido University, Sapporo 060-8628, Japan*

We theoretically study the local density of states in superconducting proximity structures where two superconducting terminals are attached to a side surface of a normal-metal wire. Using the quasiclassical Green's function method, the energy spectrum is obtained for both spin-singlet s-wave and spin-triplet p-wave junctions. In both cases, the decay length of the proximity effect at zero temperature is limited by a depairing effect due to inelastic scattering. In addition to the depairing effect, in p-wave junctions the decay length depends sensitively on the transparency at the junction interfaces, which is a unique property of odd-parity superconductors where the anomalous proximity effect occurs.

I. INTRODUCTION

The proximity effect is a phenomenon observed in a normal metal (N) attached to a superconductor (SC) [1]. Cooper pairs penetrating into an N causes superconducting-like phenomena such as the screening of magnetic fields and the suppression of the local density of states (LDOS) at the Fermi level (zero energy). The penetration length of Cooper pairs is limited by the thermal coherence length $\xi_T = \sqrt{\mathscr{D}/2\pi T}$, where $\mathscr{D}$ is the diffusion constant in the N and T is the temperature. Indeed, the Josephson current is present only when the spacing between two SCs L_1 is shorter than ξ_T [2]. Although ξ_T is the typical length scale of the proximity effect, Volkov and Takayanagi (VT) have shown that the characteristic length depends on observables [3,4]. They studied the conductance of an N wire whose side surface is connected to two superconducting terminals [see Fig. 1(b)]. The conductance depends on the phase difference of the two SCs even when $L_1 \gg \xi_T$ [3,4]. Thus this phenomenon is named the long-range phase-coherent effect.

The analysis by VT is unfortunately restricted to the weak-proximity-effect regime, where the solutions of the linearized Usadel equation describe the long-range phase-coherent effect. However, the magnitude of the proximity effect is generally sensitive to the transparency of an N/SC interface and the pairing symmetry of the SC. The strong proximity effect leads to a gaplike energy spectrum at low energy in the LDOS [5–8]. The boundary condition for the quasiclassical Green's function [9–12] enables this analysis.

Taking the essence of the circuit theory [11,12] into account, a boundary condition for the quasiclassical Usadel Green's function at an N/SC interface has been derived [13–16]. This boundary condition enables us to describe junctions of unconventional SCs such as high-T_c cuprate, spin-triplet SCs, and topological SCs. It has been well established that the Andreev bound states [17–22] (ABSs) due to the
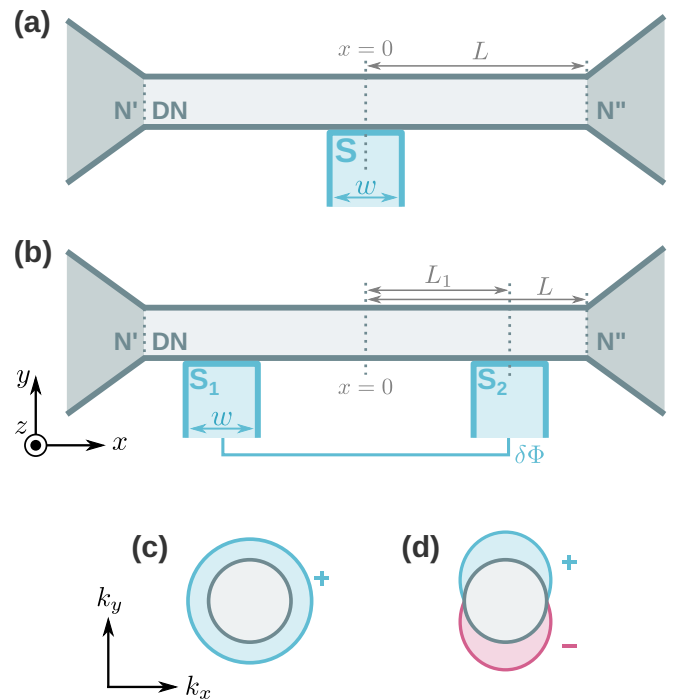

FIG. 1. Schematics of (a) T-shaped and (b) Volkov-Takayanagi (VT) junctions. The N'/DN interfaces are located at $x = \pm L$, where N' indicates an N lead. The barrier potential is present only at the S/DN interfaces. The widths and the thickness of the wires are assumed much narrower and thinner than the coherence length. The superconductor(s) is attached to the DN at $x = 0$ in (a) and at $x = \pm L_1$ (b). The superconductors have the phase difference $\delta\Phi$ in (b). Schematics of the (c) s-wave and (d) p-wave pair potentials in momentum space. The inner circles indicate the Fermi surface. The sign means the phase of the pair potential.

unconventional pairing [20] modifies the proximity effect in various ways. In an N/d-wave junction, the proximity effect can not contribute to ensemble-averaged values over random-impurity configurations [15,16]. However, the amplitude of the Josephson current in each d-wave/N/d-wave junction can exceed the ensemble-averaged Josephson current for the s-wave/N/s-wave junctions [23,24]. Spin-triplet pairings [25–36] cause several anomalies (i.e., the anomalous proximity effect) such as large zero-energy peaks in the LDOS in the N [13,14,37,38] and resonant charge transport through a dirty N [13,14,37–42]. The anomalous proximity effect is a result of the penetration of the ABSs into the N or equivalently the appearance of odd-frequency Cooper pairs in the N [40,43–55]. Such unusual phenomena have attracted much attention these days because they are equivalent to the physics of Majorana fermions appearing topologically nontrivial SCs [56–78]. At present, however, we do not know how the anomalous proximity effect modifies the long-range phase-coherent phenomena.

In this paper, we study the LDOS in a wire of a diffusive normal metal (DN) by solving numerically the quasiclassical Usadel equation in the regime of the strong proximity effect. We consider two types of proximity structures: the T-shaped junction shown in Fig. 1(a) and the VT junction shown in Fig. 1(b). We found in the T-shaped junction that the quasiparticle density of states depends strongly on the barrier potential at the junction interface. In the VT junction, the LDOS between the two superconducting electrodes depends sensitively on the phase difference of the two superconducting electrodes. In an in-phase junction, the LDOS in DN between the s-wave (p-wave) superconducting electrodes shows the zero-energy dip (peak), whereas such dip and peak structures vanish in an out-of-phase junction because of the destructive interference of Cooper pairs. In an s-wave junction, the phase-coherent effect is spatially limited by a decay length due to the depairing of Cooper pairs. In a p-wave junction, in addition to the depairing effect, the low transparency at the junction interface limits the long-range phase-coherent effect as well.

This paper is organized as following. In Sec. II, the Keldysh-Usadel formalism and the system we consider are explained. In Sec. III, we discuss the calculated LDOS for the T-shaped junction. In Sec. IV, we show the LDOS in the VT junction and discuss the long-range coherence. In particular, we focus on the junction length and depairing-ratio dependencies of the LDOS. We summarize this paper in Sec. V.

II. KELDYSH-USADEL FORMALISM

A. Usadel equation

In this paper, we consider the junctions of a DN where superconducting (S) wires are attached to a side surface of the DN as shown in Fig. 1. We refer to the junction shown in Figs. 1(a) and 1(b) as T-shaped and VT junctions, respectively. In the T-shaped junction, a narrow S wire is attached to a wire of the DN at $|x| < w/2$ and $y = 0$ with a finite interface resistance R_b, where w is the width of the S arm which is much shorter than the superconducting coherence length in the diffusive system $\xi_0 = \sqrt{\mathscr{D}/2\pi T_c}$. In the VT junction, narrow S wires are attached at $|x \mp L_1| < w/2$. The DN is

connected to lead wires of clean N at $x = \pm L$, but sufficiently narrow and thin in the y and z directions [i.e., $L_{y(z)} \ll \xi_0$].

The Green's function in the DN obeys the Usadel equation [79],

$$\mathscr{D}\nabla(\mathbb{G}\nabla\mathbb{G}) + i[\mathbb{H}, \mathbb{G}]_- = 0, \quad (1)$$

$$\mathbb{G}(\boldsymbol{r}, \varepsilon) = \begin{pmatrix} \check{g}^R(\boldsymbol{r}, \varepsilon) & \check{g}^K(\boldsymbol{r}, \varepsilon) \\ 0 & \check{g}^A(\boldsymbol{r}, \varepsilon) \end{pmatrix}, \quad (2)$$

where $\mathscr{D}$ is the diffusion constant in the DN, $\check{g}^X$ with $X = K$, R, and A are the Keyldysh, retarded, and advanced components of the Usadel Green's function, and $\mathbb{H} = \mathrm{diag}[\check{H}^R, \check{H}^A]$. Assuming the width of the DN is much narrower than ξ_0, we can ignore the spatial variation of the Green's function in the y direction in the DN. Namely, one needs to consider a quasi-one-dimensional diffusive system where the Usadel equation is reduced to

$$\mathscr{D}\partial_x(\mathbb{G}\partial_x\mathbb{G}) + i[\mathbb{H}, \mathbb{G}]_- + \mathbb{S}\Theta_S(x) = 0, \quad (3)$$

where the last term $\mathbb{S}(x, \varepsilon)$ represents effects of the S wires (see Appendix A for details). The source term $\mathbb{S}(x, \varepsilon)$ is reduced from the boundary condition in the y direction [3,4]. The steplike function is unity only at the place where the S wires are attached: $\Theta_S(x) = \Theta(w/2 - |x|)$ for the T-shaped junction and $\Theta_S(x) = \Theta(w/2 - |x - L_1|) + \Theta(w/2 - |x + L_1|)$ for the VT junction. In this paper, the symbols written in bold mean matrices in the Keldysh space, and the accents ˇ and ˆ mean matrices in particle-hole space and spin space. The identity matrices in particle-hole and spin space are respectively denoted by $\check{\tau}_0$ and $\hat{\sigma}_0$. The Pauli matrices are denoted by $\check{\tau}_j$ and $\hat{\sigma}_j$ with $j \in [1, 3]$. The Keldysh-Usadel equation is supplemented by the so-called normalization condition: $\mathbb{G}\mathbb{G} = \mathbb{1}$. The Keldysh Green's function can be obtained from the following relation:

$$\check{g}^K = \check{g}^R\check{F} - \check{F}\check{g}^A, \quad (4)$$

$$\check{F} = \check{\tau}_0 f_L + \check{\tau}_3 f_T, \quad (5)$$

where f_L and $f_T = f_T(x, \varepsilon)$ are the distribution functions which are given by $f_L = \tanh(\varepsilon/2T)$ and $f_T = 0$ in equilibrium.

The LDOS is related to the retarded and advanced components of the Usadel Green's function. The Usadel equation for $X = R$ and A is given by

$$\mathscr{D}\partial_x(\check{g}^X\partial_x\check{g}^X) + i[\check{H}^X, \check{g}^X]_- + \check{S}^X\Theta_S(x) = 0, \quad (6)$$

$$\check{g}^X(x, \varepsilon) = \begin{bmatrix} \hat{g}^X & \hat{f}^X \\ -\underset{\sim}{\hat{f}}^X & -\hat{g}^X \end{bmatrix}, \quad (7)$$

where $\check{H}^X = \varepsilon^X \check{\tau}_3$. The factor ε^X depends on X: $\varepsilon^R = \varepsilon + i\gamma$ and $\varepsilon^A = \varepsilon - i\gamma$, where ε and γ are the energy and the depairing ratio. In the Dynes formulation, we can discuss the depairing effect due to, for example, inelastic scattering by introducing γ [80–84]. In this paper, we assumed that there is no spin-dependent potential, that the Cooper pairs have one single-spin component (i.e., $\hat{\Delta} = \Delta_\mu i\hat{\sigma}_\mu\hat{\sigma}_2$ with Δ_μ being the scalar pair potential), and the phase difference between two SCs is $\delta\Phi = 0$ or π (i.e., no-current states). In this case, one

can parametrize the matrix structure of the Green's functions as follows:

$$\hat{g}^X = \hat{\sigma}_0 g^X, \tag{8}$$

$$\hat{f}^X = f_\mu^X (i\hat{\sigma}_\mu \hat{\sigma}_2), \qquad \underset{\sim}{\hat{f}}^X = f_\mu^X (i\hat{\sigma}_2 \hat{\sigma}_\mu), \tag{9}$$

where μ is related to the direction of the synthetic spin of Cooper pairs: $\mu = 0$ and $\mu = 1$–3 correspond to the spin-singlet and spin-triplet pairings. The Usadel equation can be simplified by this parametrization:

$$\mathscr{D}\partial_x(\tilde{g}^X \partial_x \tilde{g}^X) + i[\varepsilon^X \tilde{\tau}_3, \tilde{g}^X]_- + \tilde{S}^X \Theta_S(x) = 0, \tag{10}$$

$$\tilde{g}^X(x, \varepsilon) = \begin{pmatrix} g^X & f^X \\ -\underset{\sim}{f}^X & -g^X \end{pmatrix}, \tag{11}$$

where we have introduced the symbol $\tilde{\cdot}$ meaning a 2×2 matrix in spin-reduced particle-hole space [e.g., $\check{g}^X(x, \varepsilon) = \tilde{g}^X(x, \varepsilon) \otimes \hat{\sigma}_0$]. Here we assumed the phase difference between two SCs is 0 or π, which simplifies the relation between f^X and $\underset{\sim}{f}^X$ as discussed in the Appendix B.

The standard angular parametrization makes the Usadel equation much simpler [5,6,8]. The Green's function can be well parametrized by the following parameterization:

$$\tilde{g}^X = \tilde{\tau}_3 \cosh\theta + i\tilde{\tau}_2 \sinh\theta, \tag{12}$$

$$= \begin{bmatrix} \cosh\theta & \sinh\theta \\ -\sinh\theta & -\cosh\theta \end{bmatrix}, \tag{13}$$

where we omit the index X from $\theta = \theta^X(x, \varepsilon)$. This parametrization always satisfies the normalization condition: $\tilde{g}^X \tilde{g}^X = \tilde{\tau}_0$. The Usadel equation is reduced by this parametrization:

$$\mathscr{D}\frac{\partial^2\theta}{\partial x^2} + 2i\varepsilon^X \sinh\theta + \Theta_S(x)S(x, \varepsilon) = 0. \tag{14}$$

B. Effects of superconducting terminals

The last term on the left-hand side of Eq. (14) [i.e., $S(x, \varepsilon)$] represents the effect of the S arms attached to the side surface of the DN [5,8]. The typical boundary conditions [9,10] are no longer available for junctions of unconventional SCs [85]. To discuss the proximity effect by unconventional pairings, one must employ the so-called Tanaka-Nazarov condition [13,14], which is an extension of the circuit theory [11,12]. The source term S is derived from the boundary condition in the y direction. We employ the Tanaka-Nazarov boundary condition discussed in Refs. [13–16],

$$\left.\frac{d\theta}{d\bar{y}}\right|_{y=0} = \frac{R_N}{R_b \bar{L}_y}\langle F\rangle_\phi, \tag{15}$$

$$F = \frac{-2T_N(f_S \cosh\theta_0 - g_S \sinh\theta_0)}{(2 - T_N)\Xi + T_N(g_S \cosh\theta_0 - f_S \sinh\theta_0)}, \tag{16}$$

where $R_N = \rho_N L_y/L_z w$, ρ_N and R_b are the specific resistance of the DN and the interface resistance at the NS interface, $\bar{y} = y/\xi_0$, and $\bar{L}_y = L_y/\xi_0$. The angle-dependent function $T_N(\phi) = \cos^2\phi/(\cos^2\phi + z_0^2)$ is the transmission coefficient

of the N/N interface at $y = 0$ with the δ-function barrier potential $\hbar v_F z_0 \delta(y)$, ϕ is the angle of the momentum measured from the k_y axis, and $\theta_0(x) = \theta(x)|_{y=0}$. The angle ϕ is measured from the y axis. The angular bracket means angle average: $\langle\cdots\rangle_\phi \equiv (\int_{-\pi/2}^{\pi/2}\cdots\cos\phi d\phi)(\int_{-\pi/2}^{\pi/2}T_N\cos\phi d\phi)^{-1}$. The functions g_S and f_S can be obtained from the Green's functions in a homogeneous ballistic SC:

$$g_S = g_{S+} + g_{S-}, \tag{17}$$

$$f_S = \begin{cases} f_{S+} + f_{S-} & \text{for singlet SCs} \\ i(g_{S-}f_{S+} - g_{S+}f_{S-}) & \text{for triplet SCs,} \end{cases} \tag{18}$$

$$g_{S\pm}(\phi) = \frac{\varepsilon}{\sqrt{\varepsilon^2 - |\Delta_\pm|^2}}, \quad f_{S\pm}(\phi) = \frac{\Delta_\pm}{\sqrt{\varepsilon^2 - |\Delta_\pm|^2}}, \tag{19}$$

$$\Xi = 1 + g_{S+}g_{S-} - f_{S+}f_{S-}, \tag{20}$$

where the symbol X has been omitted and $\Delta_+(\phi) = \Delta_-(\pi - \phi)$. The pair potential depends on the pairing symmetry of the SC:

$$\Delta_+(\phi) = \begin{cases} \Delta_0 & \text{for an } s\text{-wave} \\ \Delta_0 \cos\phi & \text{for a } p\text{-wave,} \end{cases} \tag{21}$$

where $\Delta_0 \in \mathbb{R}$ is the amplitude of the pair potential in a homogeneous SC.

The spatial derivative in the y direction in Eq. (1) is reduced into the source term [3,4] given by

$$S(x, \varepsilon) = \frac{\mathscr{D}}{\xi_0^2}\gamma_B^{-1}\langle F(x, \varepsilon, \phi)\rangle_\phi, \tag{22}$$

where $\gamma_B = R_b\bar{L}_y^2/R_N$ is the dimensionless parameter. The parameters γ_B and z_0 can be determined independently. The interface potential z_0 determines R_b because it determines the transparency T_N, whereas γ_B determines how the effect of the SC wire is significant. In numerical simulations, it may be useful to introduce the dimensionless units: $\bar{x} = x/\xi_0$ and $\bar{\varepsilon} = \varepsilon/\Delta_0$. In this unit, the Usadel equation is reduced to

$$\frac{\partial^2\theta}{\partial\bar{x}^2} + 2i\bar{\varepsilon}\underline{\Delta}_0 \sinh\theta + \Theta_S\frac{\langle F\rangle_\phi}{\gamma_B} = 0, \tag{23}$$

where $\underline{\Delta}_0 = \Delta_0/2\pi T_c$. Equation (23) shows that the larger γ_B results in the weaker proximity effect.

The diffusivity changes the symmetry of Cooper pairs because only the isotropic s-wave pairs can survive in diffusive systems. In the present case, the symmetry of S wires determines the symmetry of the Cooper pairs induced in the DN. In the s-wave junction, spin-singlet s-wave Cooper pairs are induced, whereas spin-triplet s-wave Cooper pairs are induced in the p-wave junction [43,44]. To satisfy the Fermi-Dirac statistics, the spin-triplet Cooper pairs must belong to the odd-frequency pairing symmetry [86].

C. Boundary conditions

The Usadel Eq. (14) is supplemented by the boundary conditions. The boundary conditions for the T-shaped junction
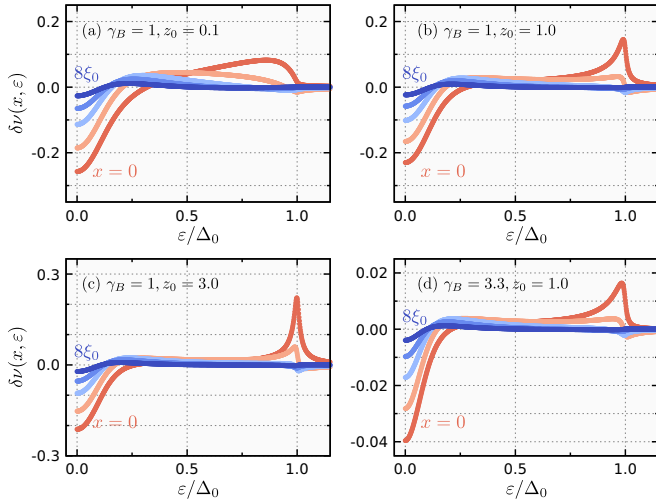
FIG. 2. Deviations of the densities of states $\delta\nu(x, \varepsilon)$ in the T-shaped junction with an s-wave superconducting wire. The results are obtained at $x = 0$, ξ_0, $2\xi_0$, $3\xi_0$, $4\xi_0$. The barrier parameter is set to $\gamma_B = 1$ in (a), (b), and (c), $\gamma_B = 3.33$ in (d). The interface-potential parameter is set to $z_0 = 0.1$ in (a), 1.0 in (b) and (d), and 3.0 in (c). The length of the DN is set to $L = 6\xi_0$. A superconductor with a width $w = 0.3\xi_0$ is attached to the DN at $x = 0$. The depairing ratio is set to $\gamma = 0.01\Delta_0$. The structures such as coherence peak and low-energy dip become sharper with increasing z_0. The amplitude becomes smaller with increasing γ_B.

and the VT junction without a phase difference are given by

$$\theta(x, \varepsilon)\Big|_{x=\pm L} = 0, \qquad \frac{d\theta(x, \varepsilon)}{dx}\Big|_{x=0} = 0. \qquad (24)$$

The boundary conditions for the VT junction with the π-phase difference is given by

$$\theta(x, \varepsilon)\Big|_{x=\pm L} = 0, \qquad \theta(x, \varepsilon)\Big|_{x=0} = 0. \qquad (25)$$

The details are written in the Appendix B.

The LDOS $\nu(x, \varepsilon)$ can be obtained from the Green's function,

$$\nu(x, \varepsilon) = \frac{\nu_0}{8} \text{Tr}[\check{\tau}_3(\check{g}^R - \check{g}^A)], \qquad (26)$$

where ν_0 is the density of states per spin at the Fermi level in the normal states. In proximity structures, it is convenient to introduce the deviation of the LDOS:

$$\delta\nu(x, \varepsilon) = \frac{\nu(x, \varepsilon) - \nu_0}{\nu_0}. \qquad (27)$$

We solve numerically Eq. (23) using the so-called forward elimination, backward substitution method.

III. T-SHAPED JUNCTIONS

We first discuss the roles of the important interface parameters (i.e., z_0 and γ_B). The deviation of the LDOS $\delta\nu(x, \varepsilon)$, which is given in Eq. (27), in the T-shaped junction with an s-wave SC are shown in Fig. 2. The deviation $\delta\nu$ is obtained at $x = 0$ (beneath the S wire), ξ_0, $2\xi_0$, $3\xi_0$, $4\xi_0$. The length
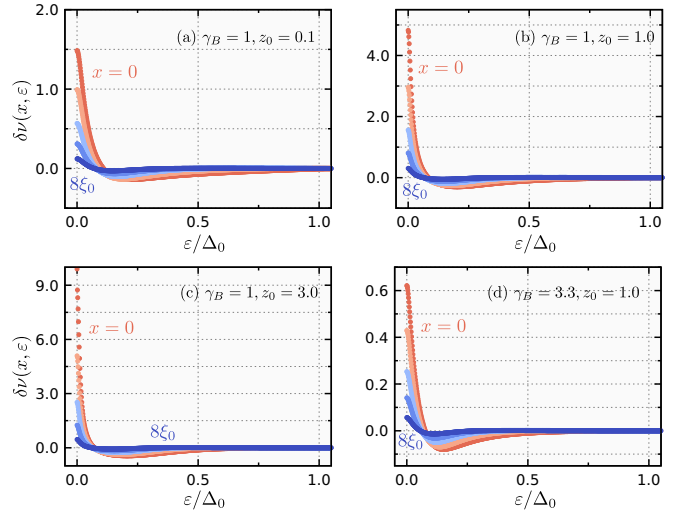

FIG. 3. Deviations of the densities of states $\delta\nu(x, \varepsilon)$ in the T-shaped junction with a p-wave SC. The parameters are set to $L = 10\xi_0$, $w = 0.3\xi_0$, and $\gamma = 0.01\Delta_0$. The zero-energy peak appears because of the p-wave nature. The zero-energy peak becomes narrower and higher with increasing the interface potential z_0.

of the DN and the width of the S arm is set to $L = 10\xi_0$ and $w = 0.3\xi_0$, respectively. The barrier parameter is set to $\gamma_B = 1$ in Figs. 2(a)–2(c), $\gamma_B = 3.33$ in (d). The interface-potential parameter is set to $z_0 = 0.1$ in Fig. 2(a), 1.0 in Figs. 2(b) and 2(d), and 3.0 in Fig. 2(c).

In an s-wave junction, the coherence peak appears beneath the S arm at the energy $\varepsilon \sim \Delta_0$ because of the proximity effect [6–8]. Simultaneously, at low energy, an energy dip [6–8,87] appears, reflecting the energy gap in the S arm [88]. The peak height and dip depth monotonically decrease with increasing the distance from the S terminal.

Comparing Figs. 2(a)–2(c), we can see that the coherence peak around $\varepsilon = \Delta_0$ becomes sharper and higher as z_0 increases. On the other hand, the dip width in the energy and real space do not strongly depends on z_0. The dip width and depth beneath the S arm are mainly determined by the spacing between normal lead wires (i.e., $2L$). We have confirmed that the low-energy dip becomes narrower with increasing system size [8]. Comparing Fig. 2(d) with 2(b), we can see that the amplitude of $\delta\nu$ becomes smaller with increasing the interface resistance (i.e., increasing of γ_B). Contrary to the s-wave case, in the T-shaped junction with a p-wave SC, the so-called zero-energy peak appears as shown in Fig. 3 due to the anomalous proximity effect by odd-frequency spin-triplet s-wave Cooper pairs [13,14,38,43] where topologically protected zero-energy states penetrate into the DN [41,42,89]. Differing from the d-wave case (not shown), the zero energy peak can survive in a p-wave junction even in a diffusive system reflecting the orbital symmetry of odd-frequency pairing [43] and the topological nature of a p-wave SC [42,52,55]. The peak becomes higher but narrower in energy space with increasing z_0. The peak width in real space, on the other hand, does not strongly depend on the z_0. As happened in the s-wave junctions, γ_B basically changes only the amplitude of the deviation $|\delta\nu|$.
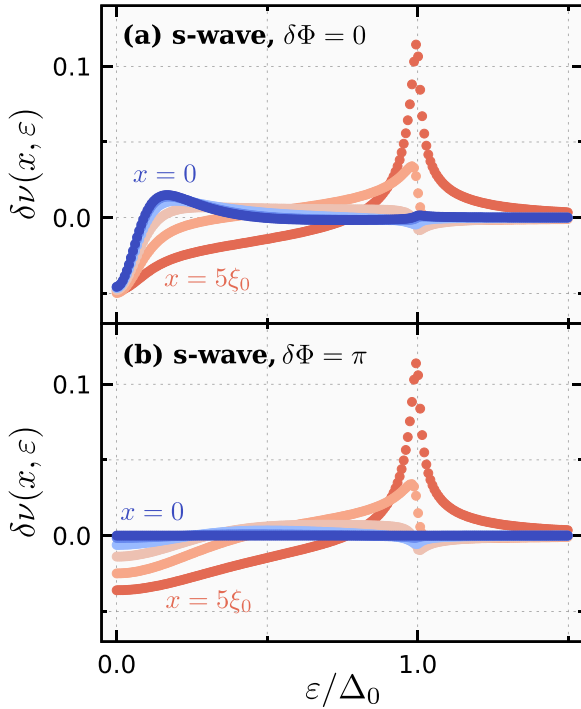
FIG. 4. Correction of the local density of states (LDOS) in the VT junction with s-wave superconducting arms. The phase difference is set to (a) $\delta\Phi = 0$ and (b) $\delta\Phi = \pi$. The results are obtained between the center of the junction (i.e., $x = 0$) and the point where a superconducting arm is attached (i.e., $x = L_1$). The parameters are set to $L = 6\xi_0$, $L_1 = 5\xi_0$, $w = 0.3\xi_0$, $\gamma = 0.01\Delta_0$, $\gamma_B = 1$, and $z_0 = 1$. The LDOS at the center of the junction is modified when $\delta\Phi = 0$, whereas the correction vanishes when $\delta\Phi = \pi$. The results mean Cooper pairs from each superconductor interfere in the DN.

The zero-energy anomaly in p-wave T-shaped junctions can be observed by the charge transport measurements [38].

In the p-wave case, the ABSs are formed at zero energy by the interference between the quasiparticles with k_y and those with $-k_y$ [22]. These ABSs penetrate into the DN because of the resonance and modify LDOS. In the present case, the large barrier potential z_0 results in the small transmission coefficient T_N, which leads to more reflected quasiparticles. As a result, the interference is enhanced and the zero-energy peak becomes higher and sharper with increasing z_0.

IV. VOLKOV-TAKAYANAGI JUNCTIONS

A. Quasiparticle spectrum

In a two-SC system such as Josephson junctions, the phase difference between the two S wires significantly affects the quasiparticle spectrum in the junction. The LDOS in the VT junction with s-wave SCs are shown in Figs. 4(a) and 4(b), where the phase difference is set to $\delta\Phi = 0$ and π, respectively. The parameters are set to $L = 6\xi_0$, $L_1 = 5\xi_0$, $w = 0.3\xi_0$, $\gamma = 0.01\Delta_0$, $\gamma_B = 1$, and $z_0 = 1$. When there is no phase difference, there is an energy dip whose size is about $0.2\Delta_0$ at the zero energy. This energy dip spreads between the S arms even though the spacing between the two arms is set to $2L_1 = 10\xi_0$.
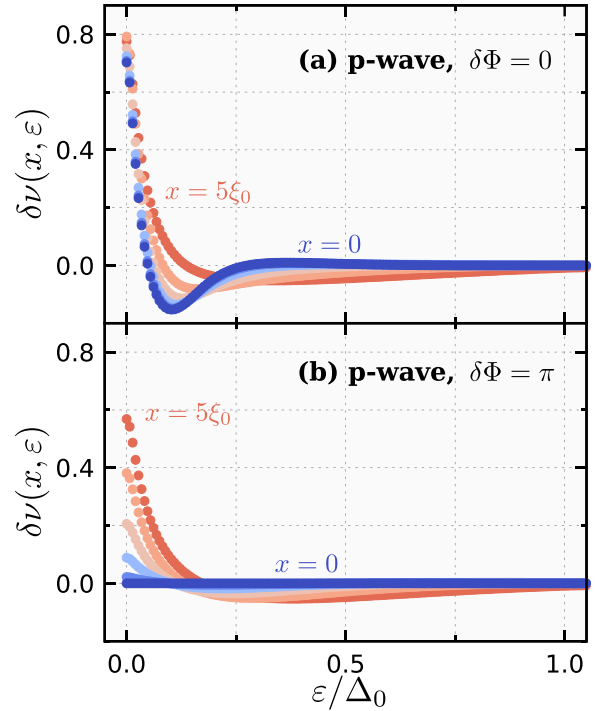

FIG. 5. LDOS in the VT junction with p-wave superconducting arms. The parameters are set to $L = 6\xi_0$, $L_1 = 5\xi_0$, $w = 0.3\xi_0$, $\gamma = 0.01\Delta_0$, $\gamma_B = 1$, and $z_0 = 1$. The parameters are set to the same values as those used in Fig. 4. The zero-energy peak spreads spatially between the two superconducting arms when $\delta\Phi = 0$, whereas it vanishes when $\delta\Phi = \pi$ because of the long-range phase coherence.

When the phase difference is $\delta\Phi = \pi$, the LDOS at the center of the junction becomes completely flat as shown in Fig. 4(b). In addition, even at intermediate points, the kink around $0.2\Delta_0$, which exists when $\delta\Phi = 0$, vanishes and $\delta\nu$ is more insensitive to ε. As a result, the energy dip is no longer prominent in Fig. 4(b). This behavior can be interpreted in terms of the destructive interference of Cooper pairs injected from the S arms. The phase of the anomalous Green's function describing the Cooper pairs is related to the sign of the pair potential. In the $\delta\Phi = \pi$ junction, the Cooper pairs from each arm have an opposite phase. In other words, the pair amplitude of Cooper pairs perfectly cancel each other at the center of a junction. As a consequence, the LDOS at the center becomes completely flat. Reflecting this behavior, the Green's function has an additional symmetry in real space $f^X(x, \varepsilon) = -f^X(x, \varepsilon)$ (see Appendix B for details).

The LDOS in the p-wave VT junctions are shown in Figs. 5(a) and 5(b), where the phase difference is set to $\delta\Phi = 0$ and π, respectively. When $\delta\Phi = 0$, the zero-energy peak spreads between the two S wires (i.e., $|x| \leqslant L_1$). The peak is the highest beneath the S wires and the lowest at the center of the junction. The low-energy dip at the center of the junction is more prominent than that beneath the S wire. The dip width at $x = 0$ is about $0.2\Delta_0$, which is comparable with that for the s-wave case shown in Fig. 4(a). When $\delta\Phi = \pi$, as happened in the s-wave VT junction, the LDOS is completely flat at $x = 0$. Moreover, the height of the zero energy peak is lower
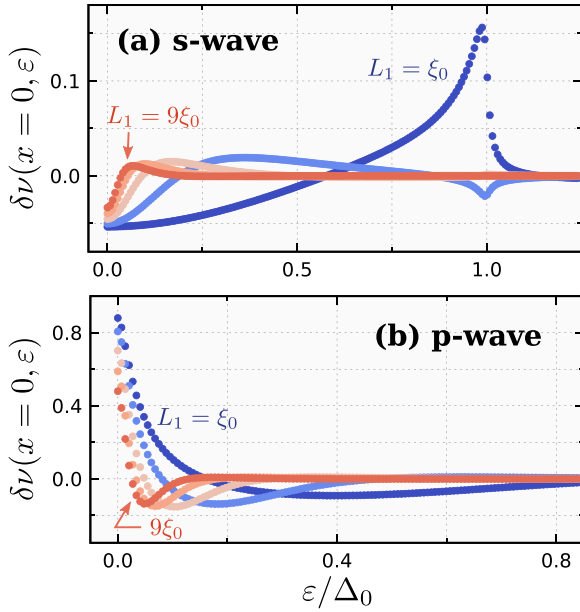
FIG. 6. Junction-length dependence of the LDOS correction at the center of VT junctions with (a) s-wave and (b) p-wave superconducting arms. The junction length is changed from $L = 2\xi_0$ to $10\xi_0$, where $\delta\Phi = 0$ and the interval between the superconducting wire and the normal lead is fixed at $L - L_1 = \xi_0$. The other parameters are set to $w = 0.3\xi_0$, $\gamma = 0.01\Delta_0$, $\gamma_B = 1$, and $z_0 = 1$.

than the $\delta\Phi = 0$ case due to the destructive interference of the Cooper pairs injected from each SC.

Differing from the typical p-wave Josephson junction [39], in the VT junction the most constructive and destructive interferences occur when $\delta\Phi = 0$ and $\delta\Phi = \pi$, respectively. As shown in Fig. 1(b), the S wires are attached to the side surface which is normal to the y axis. On the contrary, in the typical Josephson junction, p_x-wave SCs attached in the x direction. In the p-wave VT junction without a phase difference, the anomalous Green's functions injected from both of the S wires have the same sign. When the phase difference is π, however, Cooper pairs from each S wire have opposite phases, which leads to the destructive interference.

B. Junction-length dependence

The coherence is diminished with increasing the junction length. The junction-length dependence of the LDOS at the center of the VT junction with the s- and p-wave SCs are plotted in Figs. 6(a) and 6(b), respectively. In the calculations, we set the phase difference $\delta\Phi = 0$, $z_0 = 1$, and $L - L_1 = \xi_0$. In the s-wave VT junction, the LDOS shows a dip structure at low energy even in a sufficiently long junction. This energy dip becomes wider with decreasing the junction length. The height of the coherence peak around $\varepsilon = \Delta_0$ strongly depends on the junction length. With decreasing the junction length, $\delta\nu|_{\varepsilon=\Delta}$ is almost zero for $L_1 > 3\xi_0$, is negative for $L_1 = 3\xi_0$, and becomes positive for $L_1 = \xi_0$. In the short-junction limit, $\delta\nu$ becomes qualitatively the same as that in the T-shaped junction.

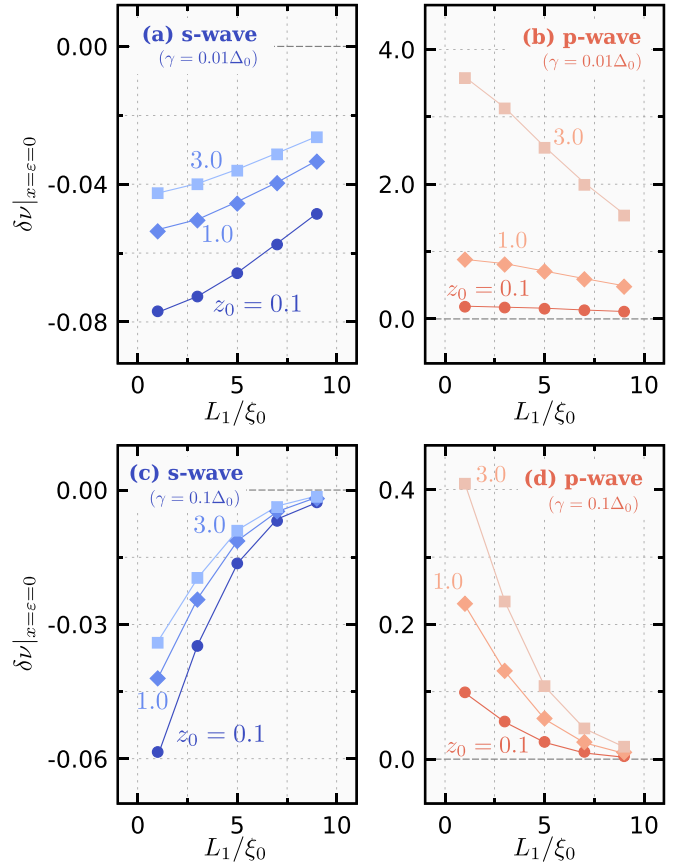The coherence in a p-wave junction modifies the LDOS, as happened in the s-wave case. As shown in Fig. 6(b), the

FIG. 7. Junction-length dependence of the LDOS at $x = 0$ and $\varepsilon = 0$. The results for the s-wave case are shown in (a) and (c), whereas those for p-wave are in (b) and (d). The depairing ratio is fixed at $\gamma = 0.01\Delta_0$ in (a) and (b), and $\gamma = 0.01\Delta_0$ in (c) and (d). The other parameters are set to $\gamma_B = 1$ and $L - L_1 = \xi_0$. In s-wave cases, the correction becomes small with increasing the barrier potential z_0, whereas it becomes large with increasing z_0. The correction decreases more rapidly with increasing L_1 when γ is large.

zero-energy peak and the energy dip can be seen even when $L = 9\xi_0$. The width of the zero-energy peak in energy space decreases monotonically with increasing the junction length. The peak height at $x = 0$ and $\varepsilon = 0$ decreases monotonically with increasing the junction length.

The junction-length dependence of the correction at $\varepsilon = 0$ and $x = 0$ (i.e., $\delta\nu|_{x=\varepsilon=0}$) in the s-wave VT junction is shown in Fig. 7(a), where the barrier parameter at the interface is set to $z_0 = 0.1$, 1.0, and 3.0, and the depairing ratio is set to $\gamma = 0.01\Delta_0$. The amplitude of the correction $|\delta\nu|$ decreases with increasing the junction length where the curvature of $|\delta\nu|$ as a function of L_1 is positive. We have confirmed that the curvature changes at a certain length. In the long-junction limit (i.e., $L_1 \gg \xi_0$), $\delta\nu|_{x=\varepsilon=0}$ approaches to 0 (i.e., normal state) where the VT junction can be regarded as a pair of two T-shaped junctions. In the p-wave junction, the amplitude of the correction $|\delta\nu|$ decreases with increasing L_1 as seen in the s-wave case. However, contrary to the s-wave case, the degree of correction decreases with increasing L_1 more rapidly when the magnitude of z_0 is large. This behavior is unique to the spin-triplet p-wave junction.
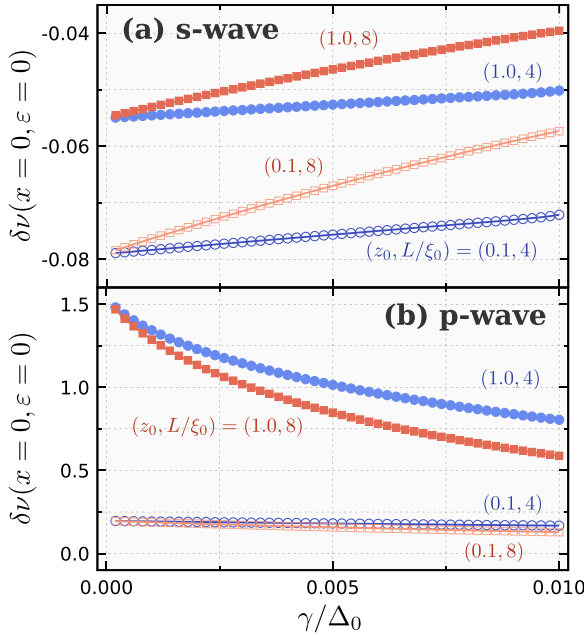
FIG. 8. Depairing-ratio dependence of the LDOS correction at $x = 0$ and $\varepsilon = 0$ for (a) an s-wave junction and (b) an p-wave junction. The interface barrier and the junction length are set to $z_0 = 1.0$ or 0.1 and $L/\xi_0 = 4$ or 8. The length L_1 is fixed to $L_1 = L - \xi_0$. The correction of the LDOS converges at a certain value regardless of the junction length, meaning that the decay length of $\delta\nu$ is determined by γ.

The junction-length dependencies with a larger depairing ratio $\gamma = 0.1\Delta_0$ are shown in Figs. 7(c) and 7(d). In both the s- and p-wave cases, the amplitudes of $\delta\nu$ are smaller and decrease more rapidly compared with the results for $\gamma = 0.01\Delta_0$. When $L_1 = 9\xi_0$, the correction $\delta\nu$ is almost zero in all of the cases. Therefore, the decay length for $|\delta\nu(x, \varepsilon = 0)|$ in the strong-proximity-effect regime would be mainly determined by $\sqrt{\mathcal{D}/\gamma}$, which is consistent with the s-wave results with the weak-proximity effect [3].

C. Depairing-ratio dependence

In real samples, depairing effects such as inelastic scattering are inevitably present. We lastly discuss the γ dependence of $\delta\nu$. The γ dependence of $\delta\nu|_{x=\varepsilon=0}$ for s- and p-wave junctions are shown in Figs. 8(a) and 8(b), respectively. The junction length and the interface barrier are fixed at $L/\xi_0 = 4$ or 8 and $z_0 = 0.1$ or 1.0. The corrections for $L/\xi_0 = 4$ and 8 approach to a certain value even though the distance between the two S electrodes are different. We therefore can conclude that the decay length of $\delta\nu$ in the VT junction is determined by γ. This behavior is consistent with that demonstrated within the weak-proximity-effect approximation [3,4]. In the s-wave case, the slopes of $\delta\nu|_{x=0,\varepsilon=0}$ curves do not strongly depends on z_0.

As shown in Fig. 8(b), the decay length of $\delta\nu$ is determined by γ in the p-wave junction as well. The corrections at $\gamma = 0.001\Delta_0$ are almost independent of the junction length, meaning the decay length for the p-wave junction is determined by the depairing ratio γ as well. Contrary to the s-wave case,
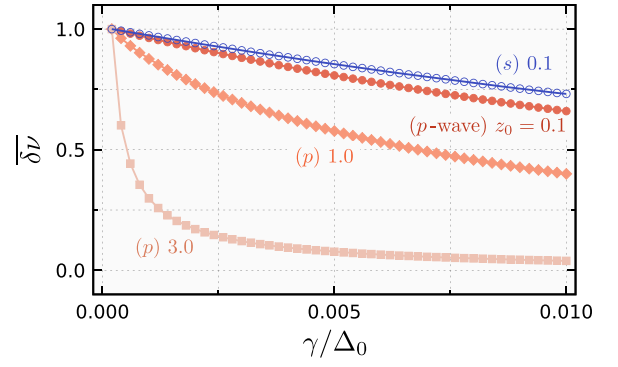

FIG. 9. Depairing-ratio dependence of the normalized correction. The normalized correction $\overline{\delta\nu}(\gamma)$ is given in Eq. (28). The parameters are set to $\gamma_B = 1$, $L = 8\xi_0$, and $L - L_1 = \xi_0$. For p-wave junctions, the correction at the zero-energy depends strongly on the interface barrier z_0 because the large barrier potential results in the high zero-energy peak.

however, the slopes for the p-wave junctions strongly depends on z_0.

We show the γ dependence of $\overline{\delta\nu}(\gamma)$ in Fig. 9, where $\overline{\delta\nu}(\gamma)$ is a function of γ normalized by its value at $\gamma = 0.001\Delta_0$;

$$\overline{\delta\nu}(\gamma) = \frac{\delta\nu(x = 0, \varepsilon = 0; \gamma)}{\delta\nu(x = 0, \varepsilon = 0; \gamma = 0.001\Delta_0)}. \quad (28)$$

We compare the following four cases: the p-wave junctions with $z_0 = 0.1$, 1.0, and 3.0 and the s-wave junction with $z_0 = 0.1$. Figure 9 clearly shows that the decay length for the p-wave junction strongly depends on z_0. The p-wave result with $z_0 = 0.1$ and the s-wave results with $z_0 = 0.1$ are not qualitatively different. Therefore, we conclude that the decay length for the p-wave junction depends on the amplitude of Cooper pairs injected by the proximity effect.

Differing from the N/DN/p-wave junction [14] where the zero-energy LDOS at the DN/p-wave interface diverges as $\propto 1/\sqrt{\gamma}$, the zero-energy correction $\delta\nu(x, \varepsilon = 0)$ does not diverge even when $\gamma \to 0$ everywhere in the DN because our system is essentially different from the system where a p-wave SC is used as an electrode [14,37].

V. CONCLUSION

We have theoretically studied the quasiparticle spectrum in a junction of a diffusive N where SCs are attached to its side surface. We have considered two types of junctions: the T-shaped junction where one SC is attached to the diffusive N and the VT junction where two SCs are attached to it. In the T-shaped junction, when the SC is spin-singlet s-wave, the LDOS, which can be measured by scanning tunneling spectroscopy measurements, has a dip structure which is consistent with the standard proximity effect. On the other hand, in the spin-triplet p-wave case, there is a zero-energy peak in the LDOS due to the anomalous proximity effect by odd-frequency pairing. The amplitude of the correction in the LDOS strongly depends on the interface barrier. In the p-wave case, in particular, the larger barrier results in the larger density of states at the zero energy.

In the VT junction, the phase difference between the two SCs significantly affects the energy spectrum. In the *s*-wave junction without a phase difference, the low-energy dip appears at the center of the junction. On the contrary, when the phase difference is π, such a low-energy dip vanishes and the LDOS at the center becomes one in the normal state because of the destructive interference of Cooper pairs. When spin-triplet *p*-wave SCs are employed instead of spin-singlet *s*-wave SCs, the zero-energy resonant states appear. When there is no phase difference, the zero-energy peak spreads spatially between the two SCs, whereas the peak vanishes at the center of the junction when the phases differ by π.

We have also studied the characteristic length scale of the phase coherence. We have shown that, in both of the *s*-wave and *p*-wave cases, the decay length of the zero-energy state is mainly characterized by the depairing ratio γ by, for example, inelastic scattering. We have demonstrated that the decay length is not simply determined by γ for spin-triplet *p*-wave junctions. The decay length for a *p*-wave junction depends also on the quality of the interface because the strength of the resonance depends strongly on the interface barrier potential.

APPENDIX A: THE SOURCE TERM OF THE USADEL EQUATION

The SC wire attached to the side surface of a DN modifies the Usadel equation in a different way from, for example, S/DN/N junctions. An important assumption in the following discussion is that the DN wire is sufficiently narrower than ξ_0, with which we can ignore the *y* and *z* dependencies of $\mathbb{G}$ in the DN. At the DN/SC interface, however, we cannot ignore the *y* dependence because the SC wire affects $\mathbb{G}$ through an interface.

The boundary condition at the interface may be described by

$$(\mathbb{G}\partial_y\mathbb{G})|_{y=0} = \mathbb{B}(x), \tag{A1}$$

where $\mathbb{B}(x)$ is calculated from $\mathbb{G}(x, y=0^+, \varepsilon)$ and $\mathbb{G}(x, y=0^-, \varepsilon) = \mathbb{G}_S(x, \varepsilon)$ with $\mathbb{G}_S(x, \varepsilon)$ being the Green's function in the SC wire. In the above equation, we ignore the *z* dependence of the Green's function because $L_z \ll \xi_0$. The Usadel equation becomes

$$\mathscr{D}\partial_x(\mathbb{G}\partial_x\mathbb{G}) + \mathscr{D}\partial_y(\mathbb{G}\partial_y\mathbb{G}) + i[\mathbb{H}, \mathbb{G}]_- = 0, \tag{A2}$$

where we have ignored the *z* dependence of $\mathbb{G}$. The spatial derivative with respect to *y* is converted into the source term through the boundary condition Eq. (A1). Since the DN wire is sufficiently narrow, the *y* dependence of $\mathbb{G}$ *in the DN* is negligible. In this case, it is useful to introduce the *y*-averaged Green's function: $\mathbb{G}'(x, \varepsilon) = \int_0^{L_y} \mathbb{G}\,dy/L_y$. The first term in Eq. (A2) becomes

$$\frac{\mathscr{D}}{L_y}\int_0^{L_y}\partial_x(\mathbb{G}\partial_x\mathbb{G})dy \approx \mathscr{D}\partial_x(\mathbb{G}'\partial_x\mathbb{G}'), \tag{A3}$$

where we assume that the *y* dependence of $\mathbb{G}(x, y, \varepsilon)$ is negligibly small. The second term in Eq. (A2) becomes

$$\frac{\mathscr{D}}{L_y}\int_0^{L_y}\partial_y(\mathbb{G}\partial_y\mathbb{G})dy = \frac{\mathscr{D}}{L_y}[\mathbb{G}\partial_y\mathbb{G}]_0^{L_y}, \tag{A4}$$

$$= -\mathscr{D}\mathbb{B}(x)/L_y, \tag{A5}$$

$$\approx -\mathscr{D}\mathbb{B}'(x)/L_y, \tag{A6}$$

where $(\mathbb{G}\partial_y\mathbb{G})|_{y=L_y} = 0$ because of the particle-conservation law. The function $\mathbb{B}'(x)$ is calculated from the *y*-averaged Green's function $\mathbb{G}'(x, \varepsilon)$ instead of $\mathbb{G}(x, y=0^+, \varepsilon)$. This assumption is valid when we can neglect the *y* dependence of $\mathbb{G}$; $L_y \ll \xi_0$.

Finally, we have the Usadel equation with a source term,

$$\mathscr{D}\partial_x(\mathbb{G}\partial_x\mathbb{G}) + i\varepsilon[\check{\tau}_3, \mathbb{G}]_- - \tilde{\Theta}(x)\frac{\mathscr{D}}{L_y}\mathbb{B}(x) = 0, \tag{A7}$$

where we have omitted the symbol $\cdot'$. When the *x* dependence of the Green's function in the SC wire is negligible, we can apply this method even when $w \sim \xi_0$. In this case, we need to regard the SC wire as a collection of narrower wires whose width is $w' \ll \xi_0$ and the source term should be calculated locally.

APPENDIX B: ADDITIONAL SYMMETRY OF THE USADEL EQUATION

In the quasiclassical formalism, the anomalous Green's functions f and $\tilde{f}$ are related by several symmetry relations. In a diffusive system (i.e., Usadel formalism), the Green's functions can have additional symmetry compared with the ballistic case.

1. General symmetry

The Usadel equation for the retarded and advanced component is given by

$$\mathscr{D}\nabla_r(\check{g}_o^X\nabla_r\check{g}_o^X) + i[\check{H}_o^X, \check{g}_o^X]_- = 0, \tag{B1}$$

$$\check{H}_o^X = \begin{bmatrix} \varepsilon^X\hat{\sigma}_0 & \hat{\Delta}(\boldsymbol{r}) \\ \hat{\Delta}^*(\boldsymbol{r}) & -\varepsilon^X\hat{\sigma}_0 \end{bmatrix}, \tag{B2}$$

$$\check{g}_o^X(\boldsymbol{r}, \varepsilon) = \begin{bmatrix} \hat{g}^X(\boldsymbol{r}, \varepsilon) & \hat{f}^X(\boldsymbol{r}, \varepsilon) \\ -\hat{\underset{\sim}{f}}^X(\boldsymbol{r}, \varepsilon) & -\hat{\underset{\sim}{g}}^X(\boldsymbol{r}, \varepsilon) \end{bmatrix}, \tag{B3}$$

where $\check{g}_o^X$ with $X = R\,(A)$ means retarded (advanced) Green's function. Assuming the single-component pair potential (i.e.,

either of the even-frequency spin-singlet or odd-frequency spin-triplet SCs), the matrix $\check{H}$ becomes

$$\check{H}_o^X = \begin{bmatrix} \varepsilon^X \hat{\sigma}_0 & \Delta_\mu(\boldsymbol{r}) i \hat{\sigma}_\mu \hat{\sigma}_2 \\ \Delta_\mu^*(\boldsymbol{r}) i \hat{\sigma}_\mu^* \hat{\sigma}_2 & -\varepsilon^X \hat{\sigma}_0 \end{bmatrix}, \quad (B4)$$

$$= \begin{bmatrix} \varepsilon^X \hat{\sigma}_0 & \Delta_\mu(\boldsymbol{r})(i \hat{\sigma}_\mu \hat{\sigma}_2) \\ \Delta_\mu^*(\boldsymbol{r})(i \hat{\sigma}_2 \hat{\sigma}_\mu) & -\varepsilon^X \hat{\sigma}_0 \end{bmatrix}. \quad (B5)$$

where $\Delta_\mu(\boldsymbol{r}) \in \mathbb{C}$ is the scalar pair potential with $\mu \in [0, 3]$. In this case, it is convenient to parametrize the spin structure of the Green's function as the following:

$$\check{g}_o^X = \begin{bmatrix} g^X \hat{\sigma}_0 & f_\mu^X (i \hat{\sigma}_\mu \hat{\sigma}_2) \\ -\underset{\sim}{f}_\mu^X (i \hat{\sigma}_2 \hat{\sigma}_\mu) & -g^X \hat{\sigma}_0 \end{bmatrix}. \quad (B6)$$

We can simplify the Usadel equation by the unitary transform. We first define the unitary matrix: $[\check{U}_1]^{-1} = \mathrm{diag}[\hat{\sigma}_0, -i \hat{\sigma}_2 \hat{\sigma}_\mu]$. Multiplying $\check{U}_1$ and $\check{U}_1^{-1}$ from the left and right side of the Usadel Eq. (B1), we have the simplified Usadel equation:

$$\mathscr{D} \boldsymbol{\nabla}_{\boldsymbol{r}} (\check{g}^X \boldsymbol{\nabla}_{\boldsymbol{r}} \check{g}^X) + i [\check{H}^X, \check{g}^X]_- = 0, \quad (B7)$$

$$\check{g}^X(\boldsymbol{r}, \varepsilon) = \begin{bmatrix} g^X & f^X \\ \underset{\sim}{f}^X & -g^X \end{bmatrix} \otimes \hat{\sigma}_0, \quad (B8)$$

$$\check{H}^X(\boldsymbol{r}, \varepsilon) = \begin{bmatrix} \varepsilon^X & \Delta(\boldsymbol{r}) \\ -\Delta^*(\boldsymbol{r}) & -\varepsilon^X \end{bmatrix} \otimes \hat{\sigma}_0, \quad (B9)$$

where we redefine the Greens functions and the matrix $\check{H}^X$ as the following: $\check{g}^X(\boldsymbol{r}, \varepsilon) = \check{U}_1 \check{g}_0^X(\boldsymbol{r}, \varepsilon) \check{U}_1^{-1}$ and $\check{H}^X(\boldsymbol{r}, \varepsilon) = \check{U}_1 \check{H}_0^X(\boldsymbol{r}, \varepsilon) \check{U}_1^{-1}$, and the subscript μ is omitted.

The matrix $\check{H}^X(x, \varepsilon)$ satisfies several symmetric relations. Hereafter, we consider the one-dimensional system. Using the Pauli matrices in the particle-hole space, we can express the matrix $\check{H}^X(x, \varepsilon)$ with a simpler form,

$$\check{H}^X(x, \varepsilon) = \check{\tau}_3 \varepsilon^X + i \check{\tau}_2 \Delta_{\mathrm{R}}(x) + i \check{\tau}_1 \Delta_{\mathrm{I}}(x), \quad (B10)$$

where $\Delta_{\mathrm{R(I)}} \in \mathbb{R}$ is the real (imaginary) part of the pair potential. The first symmetry is given by

$$\check{H}^R(x, \varepsilon) = -\check{\tau}_1 [\check{H}^A(x, \varepsilon)]^* \check{\tau}_1, \quad (B11)$$

$$g^R(x, \varepsilon) = -[g^A(x, \varepsilon)]^*, \quad (B12)$$

$$f^R(x, \varepsilon) = [\underset{\sim}{f}^A(x, \varepsilon)]^*, \quad (B13)$$

where we have used $\varepsilon^R = [\varepsilon^A]^*$. The relations above connect the retarded and advanced Green's functions. The second

symmetry is given by

$$\check{H}^X(x, \varepsilon) = \check{\tau}_1 [\check{H}^X(x, -\varepsilon)]^* \check{\tau}_1, \quad (B14)$$

$$g^X(x, \varepsilon) = [g^X(x, -\varepsilon)]^*, \quad (B15)$$

$$f^X(x, \varepsilon) = [\underset{\sim}{f}^X(x, -\varepsilon)]^*. \quad (B16)$$

The third symmetry is given by

$$\check{H}^X(x, \varepsilon) = -\check{U}_\phi [\check{H}^X(x, \varepsilon)] \check{U}_\phi, \quad (B17)$$

$$\check{U}_\phi = \begin{bmatrix} & e^{i\phi} \\ e^{-i\phi} & \end{bmatrix}, \quad (B18)$$

where $\phi(x)$ is the local phase defined as $\phi = \arctan(\Delta_{\mathrm{I}}/\Delta_{\mathrm{R}})$. We can reduce the following relations from Eq. (B17):

$$f^X(x, \varepsilon) e^{-i\phi(x)} = -\underset{\sim}{f}^X(x, \varepsilon) e^{i\phi(x)}. \quad (B19)$$

Namely, when the pair potential is a real function, we can parametrize the Green's function as

$$\check{g}^X(\boldsymbol{r}, \varepsilon) = \begin{bmatrix} g^X & f^X \\ -f^X & -g^X \end{bmatrix} \otimes \hat{\sigma}_0. \quad (B20)$$

2. Symmetry in Josephson(-ish) junctions

In Josephson(-ish) junctions, the Green's functions have additional symmetry. In this paper, we refer to the junctions in which the relation $\phi(x) = -\phi(-x)$ is satisfied as the Josephson-ish junctions (e.g., VT junctions). In other words, the real and imaginary parts of the pair potential are even and odd functions of x:

$$\Delta_{\mathrm{R}}(x) = \Delta_{\mathrm{R}}(-x), \quad (B21)$$

$$\Delta_{\mathrm{I}}(x) = -\Delta_{\mathrm{I}}(-x). \quad (B22)$$

In this case, the matrix $\check{H}^X(x, \varepsilon)$ and the Green's functions satisfy the symmetry relations related to the real space:

$$\check{H}^X(x, \varepsilon) = -\check{\tau}_1 \check{H}^X(-x, \varepsilon) \check{\tau}_1, \quad (B23)$$

$$g^X(x, \varepsilon) = g^X(-x, \varepsilon), \quad (B24)$$

$$f^X(x, \varepsilon) = -\underset{\sim}{f}^X(-x, \varepsilon). \quad (B25)$$

Combining Eqs. (B19) and (B25), we have

$$f^X(x, \varepsilon) e^{-i\phi(x)} = f^X(-x, \varepsilon) e^{i\phi(x)}. \quad (B26)$$

In particular, the relation above can further be reduced when the phase difference is either $\delta\Phi = 0$ or π:

$$\begin{aligned} f^X(x, \varepsilon) &= +f^X(-x, \varepsilon) \quad \text{for } \delta\Phi = 0, \\ f^X(x, \varepsilon) &= -f^X(-x, \varepsilon) \quad \text{for } \delta\Phi = \pi. \end{aligned} \quad (B27)$$

[1] G. Deutscher and P. G. D. Gennes, *Superconductivity* (Dekker, New York, 1969), p. 1005.

[2] P. G. DE GENNES, Rev. Mod. Phys. **36**, 225 (1964).

[3] A. F. Volkov and H. Takayanagi, Phys. Rev. Lett. **76**, 4026 (1996).

[4] A. F. Volkov and H. Takayanagi, Phys. Rev. B **56**, 11184 (1997).

[5] A. Volkov, A. Zaitsev, and T. Klapwijk, Physica C (Amsterdam) **210**, 21 (1993).

[6] A. Golubov and M. Y. Kupriyanov, J. Low Temp. Phys. **70**, 83 (1988).

[7] A. A. Golubov and M. Yu. Kupriyanov, Zh. Eksp. Teor. Fiz. **96**, 1420 (1989) [Sov. Phys. JETP **69**, 805 (1989)].

[8] A. A. Golubov, F. K. Wilhelm, and A. D. Zaikin, Phys. Rev. B **55**, 1123 (1997).

[9] A. V. Zaitsev, Zh. Eksp. Teor. Fiz. **86**, 1742 (1984) [Sov. Phys. JETP **59**, 1015 (1984)].

[10] M. Yu. Kupriyanov and V. F. Lukichev, Zh. Eksp. Teor. Fiz. **94**, 139 (1988) [Sov. Phys. JETP **67**, 1163 (1988)].

[11] Y. V. Nazarov, Phys. Rev. Lett. **73**, 1420 (1994).

[12] Y. V. Nazarov, Superlattices Microstruct. **25**, 1221 (1999).

[13] Y. Tanaka and S. Kashiwaya, Phys. Rev. B **70**, 012507 (2004).

[14] Y. Tanaka, S. Kashiwaya, and T. Yokoyama, Phys. Rev. B **71**, 094513 (2005).

[15] Y. Tanaka, Y. V. Nazarov, and S. Kashiwaya, Phys. Rev. Lett. **90**, 167003 (2003).

[16] Y. Tanaka, Y. V. Nazarov, A. A. Golubov, and S. Kashiwaya, Phys. Rev. B **69**, 144519 (2004).

[17] L. J. Buchholtz and G. Zwicknagl, Phys. Rev. B **23**, 5788 (1981).

[18] J. Hara and K. Nagai, Prog. Theor. Phys. **76**, 1237 (1986).

[19] C. R. Hu, Phys. Rev. Lett. **72**, 1526 (1994).

[20] Y. Tanaka and S. Kashiwaya, Phys. Rev. Lett. **74**, 3451 (1995).

[21] S. Kashiwaya and Y. Tanaka, Rep. Prog. Phys. **63**, 1641 (2000).

[22] Y. Asano, Y. Tanaka, and S. Kashiwaya, Phys. Rev. B **69**, 134501 (2004).

[23] Y. Asano, Phys. Rev. B **64**, 014511 (2001).

[24] Y. Asano, Y. Tanaka, T. Yokoyama, and S. Kashiwaya, Phys. Rev. B **74**, 064507 (2006).

[25] B. S. Shivaram, T. F. Rosenbaum, and D. G. Hinks, Phys. Rev. Lett. **57**, 1259 (1986).

[26] C. H. Choi and J. A. Sauls, Phys. Rev. Lett. **66**, 484 (1991).

[27] Y. Maeno, H. Hashimoto, K. Yoshida, S. Nishizaki, T. Fujita, J. Bednorz, and F. Lichtenberg, Nature **372**, 532 (1994).

[28] T. M. Rice and M. Sigrist, J. Phys.: Condens. Matter **7**, L643 (1995).

[29] K. Ishida, H. Mukuda, Y. Kitaoka, K. Asayama, Z. Mao, Y. Mori, and Y. Maeno, Nature **396**, 658 (1998).

[30] M. J. Graf, S.-K. Yip, and J. A. Sauls, Phys. Rev. B **62**, 14393 (2000).

[31] S. Saxena, P. Agarwal, K. Ahilan, F. Grosche, R. Haselwimmer, M. Steiner, E. Pugh, I. Walker, S. Julian, P. Monthoux *et al.*, Nature **406**, 587 (2000).

[32] D. Aoki, A. Huxley, E. Ressouche, D. Braithwaite, J. Flouquet, J.-P. Brison, E. Lhotel, and C. Paulsen, Nature **413**, 613 (2001).

[33] A. P. Mackenzie and Y. Maeno, Rev. Mod. Phys. **75**, 657 (2003).

[34] N. T. Huy, A. Gasparini, D. E. de Nijs, Y. Huang, J. C. P. Klaasse, T. Gortenmulder, A. de Visser, A. Hamann, T. Görlach, and H. v. Löhneysen, Phys. Rev. Lett. **99**, 067006 (2007).

[35] S. Kashiwaya, H. Kashiwaya, H. Kambara, T. Furuta, H. Yaguchi, Y. Tanaka, and Y. Maeno, Phys. Rev. Lett. **107**, 077003 (2011).

[36] Y. Machida, A. Itoh, Y. So, K. Izawa, Y. Haga, E. Yamamoto, N. Kimura, Y. Onuki, Y. Tsutsumi, and K. Machida, Phys. Rev. Lett. **108**, 157002 (2012).

[37] Y. Tanaka, Y. Asano, A. A. Golubov, and S. Kashiwaya, Phys. Rev. B **72**, 140503(R) (2005).

[38] Y. Asano, Y. Tanaka, A. A. Golubov, and S. Kashiwaya, Phys. Rev. Lett. **99**, 067005 (2007).

[39] Y. Asano, Y. Tanaka, and S. Kashiwaya, Phys. Rev. Lett. **96**, 097007 (2006).

[40] Y. Asano and Y. Tanaka, Phys. Rev. B **87**, 104513 (2013).

[41] S. Ikegaya, Y. Asano, and Y. Tanaka, Phys. Rev. B **91**, 174511 (2015).

[42] S. Ikegaya, S.-I. Suzuki, Y. Tanaka, and Y. Asano, Phys. Rev. B **94**, 054512 (2016).

[43] Y. Tanaka and A. A. Golubov, Phys. Rev. Lett. **98**, 037003 (2007).

[44] Y. Tanaka, A. A. Golubov, S. Kashiwaya, and M. Ueda, Phys. Rev. Lett. **99**, 037005 (2007).

[45] Y. Tanaka, Y. Tanuma, and A. A. Golubov, Phys. Rev. B **76**, 054522 (2007).

[46] M. Eschrig, T. Löfwander, T. Champel, J. Cuevas, and G. Schön, J. Low Temp. Phys. **147**, 457 (2007).

[47] Y. Asano, Y. Tanaka, and A. A. Golubov, Phys. Rev. Lett. **98**, 107002 (2007).

[48] Y. Asano, A. A. Golubov, Y. V. Fominov, and Y. Tanaka, Phys. Rev. Lett. **107**, 087001 (2011).

[49] T. Yokoyama, Y. Tanaka, and N. Nagaosa, Phys. Rev. Lett. **106**, 246601 (2011).

[50] S. Higashitani, H. Takeuchi, S. Matsuo, Y. Nagato, and K. Nagai, Phys. Rev. Lett. **110**, 175301 (2013).

[51] S.-I. Suzuki and Y. Asano, Phys. Rev. B **89**, 184508 (2014).

[52] S.-I. Suzuki and Y. Asano, Phys. Rev. B **91**, 214510 (2015).

[53] Y. Asano and A. Sasaki, Phys. Rev. B **92**, 224508 (2015).

[54] S. Ikegaya and Y. Asano, J. Phys.: Condens. Matter **28**, 375702 (2016).

[55] S.-I. Suzuki and Y. Asano, Phys. Rev. B **94**, 155302 (2016).

[56] N. Read and D. Green, Phys. Rev. B **61**, 10267 (2000).

[57] D. A. Ivanov, Phys. Rev. Lett. **86**, 268 (2001).

[58] X.-L. Qi and S.-C. Zhang, Rev. Mod. Phys. **83**, 1057 (2011).

[59] L. Fu and C. L. Kane, Phys. Rev. Lett. **100**, 096407 (2008).

[60] Y. Tanaka, T. Yokoyama, and N. Nagaosa, Phys. Rev. Lett. **103**, 107002 (2009).

[61] L. Fu and C. L. Kane, Phys. Rev. Lett. **102**, 216403 (2009).

[62] A. R. Akhmerov, J. Nilsson, and C. W. J. Beenakker, Phys. Rev. Lett. **102**, 216404 (2009).

[63] J. D. Sau, R. M. Lutchyn, S. Tewari, and S. Das Sarma, Phys. Rev. B **82**, 094522 (2010).

[64] Y. Tanaka, M. Sato, and N. Nagaosa, J. Phys. Soc. Jpn. **81**, 011013 (2012).

[65] T. Mizushima, Y. Tsutsumi, M. Sato, and K. Machida, J. Phys.: Condens. Matter **27**, 113203 (2015).

[66] M. Sato and S. Fujimoto, J. Phys. Soc. Jpn. **85**, 072001 (2016).

[67] T. Mizushima, Y. Tsutsumi, T. Kawakami, M. Sato, M. Ichioka, and K. Machida, J. Phys. Soc. Jpn. **85**, 022001 (2016).

[68] M. Sato and Y. Ando, Rep. Prog. Phys. **80**, 076501 (2017).

[69] I. van Weperen, B. Tarasinski, D. Eeltink, V. S. Pribiag, S. R. Plissard, E. P. A. M. Bakkers, L. P. Kouwenhoven, and M. Wimmer, Phys. Rev. B **91**, 201413(R) (2015).

[70] J. Shabani, M. Kjaergaard, H. J. Suominen, Y. Kim, F. Nichele, K. Pakrouski, T. Stankevic, R. M. Lutchyn, P. Krogstrup, R. Feidenhans'l, S. Kraemer, C. Nayak, M. Troyer, C. M. Marcus, and C. J. Palmstrøm, Phys. Rev. B **93**, 155402 (2016).

[71] R. Lutchyn, E. Bakkers, L. Kouwenhoven, P. Krogstrup, C. Marcus, and Y. Oreg, Nat. Rev. Mater. **3**, 52 (2018).

[72] R. S. Deacon, J. Wiedenmann, E. Bocquillon, F. Domínguez, T. M. Klapwijk, P. Leubner, C. Brüne, E. M. Hankiewicz, S. Tarucha, K. Ishibashi, H. Buhmann, and L. W. Molenkamp, Phys. Rev. X **7**, 021011 (2017).

[73] S. Gazibegovic, D. Car, H. Zhang, S. C. Balk, J. A. Logan, M. W. de Moor, M. C. Cassidy, R. Schmits, D. Xu, G. Wang *et al.*, Nature **548**, 434 (2017).

[74] Ö. Gül, H. Zhang, J. D. Bommer, M. W. de Moor, D. Car, S. R. Plissard, E. P. Bakkers, A. Geresdi, K. Watanabe, T. Taniguchi, and L. P. Kouwenhoven, Nat. Nanotechnol. **13**, 192 (2018).

[75] J. E. Sestoft, T. Kanne, A. N. Gejl, M. von Soosten, J. S. Yodh, D. Sherman, B. Tarasinski, M. Wimmer, E. Johnson, M. Deng, J. Nygård, T. S. Jespersen, C. M. Marcus, and P. Krogstrup, Phys. Rev. Mater. **2**, 044202 (2018).

[76] J. Chen, P. Yu, J. Stenger, M. Hocevar, D. Car, S. R. Plissard, E. P. Bakkers, T. D. Stanescu, and S. M. Frolov, Sci. Adv. **3**, e1701476 (2017).

[77] S.-I. Suzuki, Y. Kawaguchi, and Y. Tanaka, Phys. Rev. B **97**, 144516 (2018).

[78] L. A. B. Olde Olthof, S.-I. Suzuki, A. A. Golubov, M. Kunieda, S. Yonezawa, Y. Maeno, and Y. Tanaka, Phys. Rev. B **98**, 014508 (2018).

[79] K. D. Usadel, Phys. Rev. Lett. **25**, 507 (1970).

[80] R. C. Dynes, V. Narayanamurti, and J. P. Garno, Phys. Rev. Lett. **41**, 1509 (1978).

[81] A. Mikhailovsky, S. Shulga, A. Karakozov, O. Dolgov, and E. Maksimov, Solid State Commun. **80**, 511 (1991).

[82] Y. Noat, V. Cherkez, C. Brun, T. Cren, C. Carbillet, F. Debontridder, K. Ilin, M. Siegel, A. Semenov, H.-W. Hübers, and D. Roditchev, Phys. Rev. B **88**, 014503 (2013).

[83] P. Szabó, T. Samuely, V. Hašková, J. Kačmarčík, M. Žemlička, M. Grajcar, J. G. Rodrigo, and P. Samuely, Phys. Rev. B **93**, 014505 (2016).

[84] F. Herman and R. Hlubina, Phys. Rev. B **95**, 094514 (2017).

[85] The boundary condition (BC) for the quasiclassical Green's function was first derived by A.V. Zaitsev [9]. However, this BC is valid only for ballistic junctions (i.e., Eilenberger formalism). Afterward, Zaitsev BC was extended to the Usadel Green's function [10] with which one can describe phenomena in diffusive systems with s-wave SCs. This BC was further extended to junctions with unconventional (and topological) SCs [13,14] (e.g., high-T_c SCs, heavy-fermion compounds, and Sr_2RuO_4). Namely, one can discuss DN/unconventional-SC junctions *only* by using so-called Tanaka-Nazarov BC.

[86] V. L. Berezinskii, Pis'ma Zh. Eksp. Teor. Fiz. **20**, 628 (1974) [JETP Lett. **20**, 287 (1974)].

[87] A. Keles, A. V. Andreev, and B. Z. Spivak, Phys. Rev. B **89**, 014505 (2014).

[88] We have confirmed that the anomalous Green's function becomes purely imaginary, meaning that the conventional even-frequency Cooper pairs are injected from the SC to the diffusive normal metal.

[89] We have confirmed that the anomalous Green's function becomes a real function, meaning that the odd-frequency Cooper pairs are induced.